

## MONITORING TRIDIMENSIONAL SOIL SALINITY PATTERNS AT THE FIELD SCALE USING ELECTROMAGNETIC INDUCTION SENSING AND INVERSION

J.L. Gómez Flores<sup>1</sup>, M. Ramos Rodríguez<sup>1</sup>, A. González Jiménez<sup>1</sup>, M. Farzadian<sup>2</sup>, J.F. Herencia Galán<sup>3</sup>, B. Salvatierra Bellido<sup>4</sup>, P. Cermeño Sacristan<sup>3</sup>, K.Vanderlinden<sup>1</sup>

<sup>1</sup>IFAPA Centro Alameda del Obispo, Córdoba, Spain.

<sup>2</sup>Instituto Nacional de Investigação Agrária e Veterinária, Oeiras, Portugal.

<sup>3</sup>IFAPA Centro Las Torres, Alcalá del Río (Seville), Spain.

<sup>4</sup>IFAPA Centro Rancho de la Merced, Jerez de la Frontera, Spain.

**ABSTRACT.** Continuous monitoring of soil salinity/sodicity is essential in environments such as the B-XII irrigation district (SW Spain) where a shallow saline water table and intensive irrigated agriculture create a fragile equilibrium between salt accumulation and leaching in the topsoil. We evaluate to which extent electromagnetic induction (EMI) sensing and inversion with limited calibration can be used to accomplish such monitoring purposes.

EMI surveys were performed in 2017 and 2020 in a field with a heavy clay soil. Soil samples were taken at different locations and depths along a transect and analyzed for salinity/sodicity-related parameters. Inversion of the EMI signals along the transect yielded consistent conductivity images for both years and showed a good relation ( $R^2=0.80$ ) with these parameters.

Our results show that inversion of EMI signals offers a powerful means for monitoring spatial and temporal changing soil salinity/sodicity for the specific conditions of the B-XII irrigation district.

**RESUMEN.** El monitoreo continuo de la salinidad/sodicidad del suelo es esencial en entornos como el distrito de riego B-XII (suroeste de España) donde un nivel freático salino poco profundo y la agricultura de regadío intensivo crean un frágil equilibrio entre la acumulación de sales y la lixiviación en la capa superficial del suelo. Evaluamos las limitaciones de la detección e inversión de inducción electromagnética (EMI) para lograr este propósito.

Las mediciones EMI se realizaron en 2017 y 2020 en una parcela de suelo muy arcilloso. Se tomaron muestras de suelo en diferentes lugares y profundidades a lo largo de un transecto y se analizaron para determinar los parámetros relacionados con salinidad/sodicidad. La inversión EMI en el transecto arrojó imágenes de conductividad consistentes para ambos años y mostró buena relación ( $R^2 = 0.80$ ) con estos parámetros.

Nuestros resultados muestran que la inversión de señales EMI ofrece un método potente para monitorear cambios espacio-temporales en la salinidad/sodicidad del suelo para las condiciones específicas del distrito de riego B-XII.

### 1.- Introduction

Soil salinization/sodification represents a latent threat to soil quality and agricultural sustainability in regions where proper agricultural management in response to specific environmental conditions has enabled the development of a fragile balance between salt buildup and removal rates. Potentially changing climate conditions, short-term fluctuations in irrigation water availability and quality, and saline water table depth, or changes in the soil and water management might disrupt this equilibrium with negative consequences for crop production and soil functionality (e.g. Assouline et al., 2015; Hopmans et al., 2021).

To keep track of the soil salinity status in such environments a growing demand for efficient field monitoring methods exists. Yet, conventional soil monitoring entails periodical soil sampling and laboratory analysis (Corwin and Yemoto, 2017) which are time-consuming, labor-intensive and expensive. In addition, the measurements cannot be repeated at the same locations since the soil sampling procedure is destructive. Alternatively, networks of permanently installed electromagnetic sensors can be used to measure soil moisture, temperature and bulk electrical conductivity at fixed depths. Although such an approach yields quasi-continuous measurements in time, it provides only limited spatial information at the locations where sensors are installed.

Detailed spatial soil information can be obtained through electromagnetic induction (EMI) sensing, which has become one of the most popular methods for characterizing the spatial variability of soils and their properties and states at the field scale (e.g. Doolittle and Brevik, 2014; Pedrera-Parrilla et al., 2016), since it is fast and easy to deploy in the field mainly due to its non-contact and non-invasive nature and its large measurement support volumes ( $\sim m^3$ ). This technique allows the simultaneous measurement of the integrated apparent electrical conductivity (ECa) measured across different soil depths. Under non-saline soil conditions, the ECa is usually related with clay content and soil water content, among other soil properties, while under saline conditions it is the contribution of the solute concentration of the soil water that dominates the ECa signal. When integrated in a mobile measurement platform, these instruments can scan large areas and take thousands

of measurements within a couple of hours. The georeferenced ECa data are then mapped and related with independent measurements of the relevant soil properties for calibration (Triantafylis et al., 2000; Nogués et al., 2006; Corwin and Scudiero, 2016).

Yet, this approach does not directly provide information on the vertical distribution of the “true” soil conductivity (EC) and the related soil properties. Recent methodological advances in hydrogeophysics (Binley et al., 2015) are unlocking the full potential of EMI through joint inversion of multi-receiver data (Triantafylis and Monteiro Santos, 2013; McLachlan et al., 2021) by estimating the vertical distribution of EC across the soil profile, from which soil salinity profiles can be estimated in 2D and quasi-3D (Jadoon et al., 2015; Zare et al., 2015; Koganti et al., 2018; Farzaman et al., 2019; Paz et al. 2020).

In this work we evaluate the potential of EMI tomography for mapping changes in salinity/sodicity between 2017 and 2020 in the reclaimed marsh soils of a commercial field in the B-XII irrigation district in SW Spain. The specific objectives are (1) to provide robust calibration equations to estimate the saturated paste extract conductivity (ECe) and the exchangeable sodium percentage (ESP) from EC using minimal soil analysis data and (2) to map the change in soil salinity/sodicity status between both years at different depths.

## 2.- Material and Methods

### 2.1. Site description

This study was performed in a 4-ha commercial field in the B-XII irrigation district (Lebrija, Seville) (Fig.1), where a flourishing agriculture has developed since the early eighties on the reclaimed saline marsh soils. The area is characterized by an artificially drained shallow saline water table and a rather homogeneous heavy clay soil texture (Moreno et al., 1981; Dominguez et al., 2001). The drainage system in the field consisted of 0.3-m long ceramic sections that form parallel 250-m long pipes, buried at a depth of 1 m and separated by a distance of 10 m. The pipes discharge into a drainage channel along the northern limit of the field.



Fig.1. Study site location.

The climate of the zone is typically Mediterranean, with moderate humid winters and hot dry summers. Annual rainfall ranges from 350 to 1100 mm, with an average of 550 mm. Most of the precipitation falls from November to March. There is practically no rainfall during July and

August. Annual reference evapotranspiration is about 1000 mm on average.

In 2017, the total rainfall between 1 Sept. and the EMI survey day, 21 Nov. (81 days), was 140 mm of which about one third was measured the week before the EMI survey. In contrast, for survey in 2020, total rainfall since 1 Sept. 2019 was 180 mm, distributed over a period twice as long as compared to 2017. The EMI measurement in 2020 was preceded by a long dry period and a smaller amount of rainfall just before the EMI measurement. Therefore, the soil profile is expected to be wetter in 2017 than 2020, as observed also during the soil sampling on both days.

### 2.2. EMI measurements

Electromagnetic induction surveys were conducted in November 2017 and February 2020 using a DualEM21S (DualEM Inc., Milton, ON, Canada). This instrument contains dual-geometry receivers (horizontal, HCP/perpendicular, PRP) at 1 and 2 m from the transmitter and allows simultaneous conductivity sounding down to theoretical depths of exploration near 0.5, 1, 1.5 and 3m.

The sensor is operated at a height of 0.105 m above the soil surface in a customized polyvinyl chloride (PVC) sled towed by an all-terrain vehicle (ATV). A real-time kinematic differential global positioning system (Trimble, Sunnyvale, CA, USA) is used for georeferencing the EMI measurements. EMI data and coordinates are logged on a mesa3 field computer (Juniper Systems, Logan, UT, USA).

Due to hardware configuration problems only the PRP2 (1 m) and HCP2 (3 m) signals were logged during the survey in 2017. In 2017 measurements were performed in the direction of the drainage pipes and in the perpendicular direction. In 2020 measurements were only performed in the former direction since the field was ridged and not transitable in the perpendicular direction.

### 2.3. Soil sampling and laboratory analysis

On both survey dates soil samples were taken at 5 locations along a transect parallel to the drainage pipes (Fig. 2), with 0.2-m depth increments down to 1 m, using a 0.05-m diameter Edelman soil auger. The 25 soil samples obtained on each date were air dried ground and passed through a 2 mm sieve. Saturated soil pastes were prepared according to the standard method (Rhoades 1982), adding deionized water to 200 g of air-dried soil and allowing the sample to reach equilibrium during 24. Subsequently, the extracts were collected and ECe and pH was measured using a conductivity/pH meter (Hanna Instruments, HI5521). The extracts were analyzed for Na<sup>+</sup>, K<sup>+</sup>, Mg<sup>2+</sup>, and Ca<sup>2+</sup> using an inductively coupled Plasma Optical Emission Spectrometry (ICP-OES) (Perkin Elmer Avio 200), for nitrate (NO<sub>3</sub><sup>-</sup>) using an ion-selective electrode (IMACIMUS Multi ION), for Cl<sup>-</sup> an argentometric method (APHA, 1989; Mohr Method, 4500 Cl- B) and an automatic titrator (Mettler Toledo T70); and for sulfate (SO<sub>4</sub><sup>2-</sup>) using a turbidimetric method (APHA, 1989,

Method 4500 SO<sub>4</sub>= E) and spectrophotometer UV-VIS (Varian Cary 50).

EC and pH for soil samples was also measured in a 1:2.5 aqueous extract.

Sodium adsorption ratio (SAR) was computed as  $SAR = [Na^+]/\left(\frac{[Ca^{2+}] + [Mg^{2+}]}{2}\right)^{0.5}$ , with the cation concentration in meq L<sup>-1</sup>. The exchangeable sodium percentage (ESP) was estimated using  $ESP = 1.475 SAR/[1 + 0.0147 SAR]$  (U.S. Salinity Laboratory Staff, 1954).

#### 2.4. Data processing, inversion and salinity/sodicity classification

Raw georeferenced EMI measurements were corrected for positional error caused by delays in data transmission, reception or logging during the field measurement according to the method proposed by González Jiménez et al. (2021, this issue). The coordinate correction was performed using a time-lag of 1.45 s and 1.55 s for the signals PRP2/HCP2 resulting in a translation of 2.65 m and 2.83 m for PRP2/HCP2, respectively. Before applying this coordinate correction procedure spatially inconsistent and erroneous EMI (or ECa) measurements were removed from the dataset.

The spatial data were interpolated on a 0.5 × 0.5 m grid using the inverse distance method as implemented in Surfer (Golden Software, LLC Boulder, CO) and descriptive statistics were calculated and compared for the surveys of 2017 and 2020.

To estimate the vertical distribution of the electrical conductivity (EC) the four EMI signals were inverted using the EM4Soil software (EMTOMO, Lisbon). EM4Soil estimates pseudo-bidimensional images of the EC distribution across the soil profile, conditioned on the neighboring ECa values. According to the imposed smoothness condition for the estimation of the EC profile, two inversion algorithms are considered (S1 y S2). Both are variations of the Occam regularization method (de Groot-Hedlin and Constable, 1990), being the inversion algorithm S2 the one used in this study since it produced smoother results than S1. More details about the inversion algorithm can be found in Triantafyllis y Monteiro Santos (2013). 2D inversions were performed along the transect while 3D inversions for 2017 and 2020 were performed for the entire field, from which maps of EC were obtained for the different sampling depths: 0.1, 0.3, 0.5, 0.7 and 0.9 meters.

The EC values were then converted to ECe and ESP using calibration equations with the analytical soil data. LOOCV is a cross-validation method that calculates as many models as there are observations. The model was fitted each time with all the observations except one, which is used to evaluate the model. The "caret" package from R has been used for the calculation (Kuhn et al., 2020). The resulting maps were categorized according to the criteria of the American salinity/sodicity soil classification, distinguishing 4 zones: Non-saline and non-sodic if ECe <

4 dS/m and ESP < 15%, sodic if ECe < 4 dS/m and ESP > 15%, saline-sodic if 4 < ECe < 8 dS/m and ESP > 15%, and highly saline-sodic if ECe > 8 dS/m and ESP > 15%.

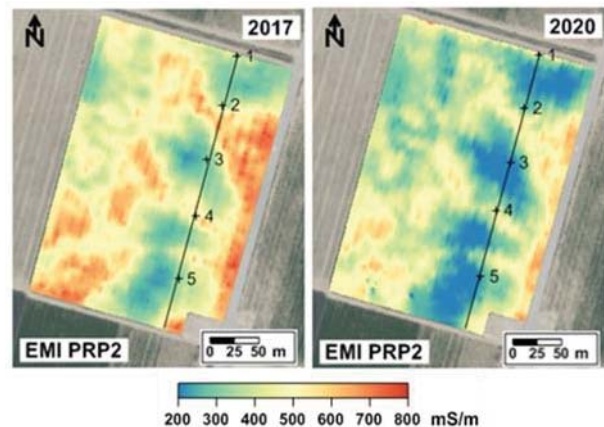


Fig. 2. Maps of EMI signals (ECa values) and location of the sampling points along the transect for the surveys of 2017 and 2020.

### 3.- Results and Discussion

#### 3.1. EMI measurements in 2017 and 2020

The average PRP2 and HCP2 signals were 26 and 17 % larger in 2017 than in 2020, respectively, indicating overall more conductive conditions in 2017 (Table 1). In 2017 and 2020 the PRP2/HCP2 ratio was 1.2 and 1.3, respectively, indicating a slightly less homogeneous conductivity across the soil profile in 2017. The spatial variability (CV) was larger in 2020 for both signals which points towards a more homogeneous conductivity across the field in 2017. For both surveys the CV was smaller for the deep signal (HCP2) than for the shallow signal (PRP2), indicating a more homogenous conductivity distribution in the subsoil than in the topsoil.

Table 1. Descriptive statistics of the interpolated EMI signals (mS/m).

	PRP2 2017	PRP2 2020	HCP2 2017	HCP2 2020
m*	474.0	376.0	566.8	484.2
min	204.9	96.1	337.1	266.3
max	831.0	753.1	790.0	780.7
med	477.5	376.3	574.4	491.1
s	118.7	109.3	98.3	100.0
CV	0.25	0.29	0.17	0.21
Curt.	-0.826	-0.779	-0.885	-0.866
Skewn.	0.019	0.128	-0.185	-0.121

\*m: mean; med: median; s: standard deviation; CV: coefficient of variation

#### 3.2. Temporal evolution of EMI

Fig. 3a shows the increment of the PRP2 signal from 2017 to 2020 ( $\Delta PRP2 = PRP2_{2020} - PRP2_{2017}$ ). The smallest increments (near zero) were observed in the areas with the lowest PRP2 values as also confirmed by Fig. 3b where the deviation from the 1:1 line is largest for the largest PRP2

values. The histogram and cumulative probability curve of  $\Delta PRP2$  (Fig. 3c) shows that PRP2 decreased from 2017 to 2020 in most of the field. At about 50 % of the pixels PRP2 decreased by more than 100 mS/m from 2017 to 2020.

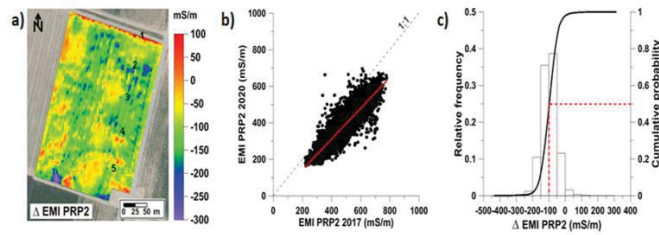


Fig. 3. a) Increments of the PRP2 signals from 2017 to 2020, b) scatter plot and deviation from 1:1 line, and c) histogram of increments and cumulative probability.

### 3.3. Inversion of EMI datasets

Fig. 4a and Fig. 4b show the EC images of the soil profile along the transect (Fig. 2) for 2017 and 2020, respectively. The most visible differences between both surveys are observed in the top 0.5 m of the soil profile, with larger zones of small EC in 2020. However, the strongest absolute increments are found below 0.5 m. (Fig. 4c).

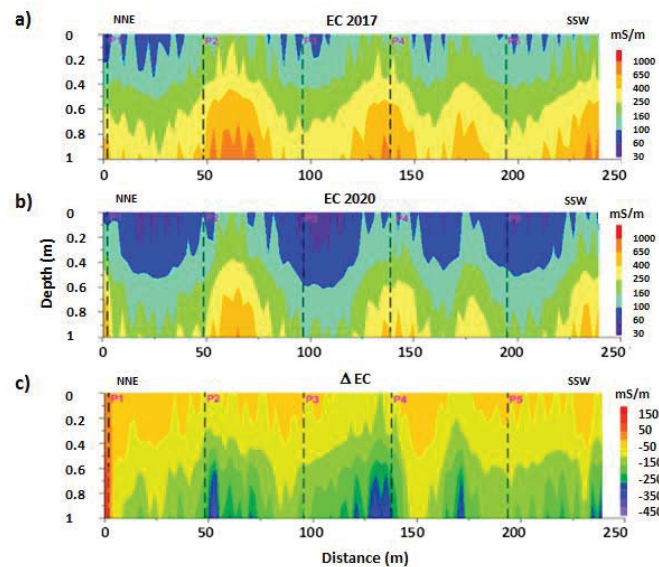


Fig. 4. a) Inverted ECa (EC) profile along the transect for 2017, b) 2020, and c) increments between 2017 and 2020 ( $\Delta EC = EC_{2020} - EC_{2017}$ ).

The relationships between inverted ECa and ECe for 2017 and 2020 (Fig. 5) show that although EC values were higher in 2017 than in 2020, ECe shows a different tendency, with higher ECe at intermediate depths in certain points. These apparently different relationships for EC and ECe between 2017 and 2020 show in this case the predominant effect of variations in soil water versus salt content on the EMI measurements.

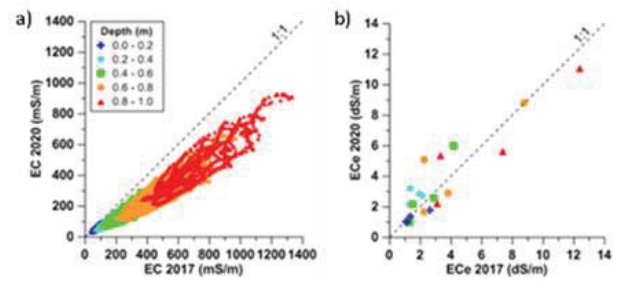


Fig. 5. Relationships between a) EC and b) ECe for 2017 and 2020.

### 3.4. Correlation between EC and analytical soil parameters

As expected, ECe and ESP increased with depth (Table 2). Overall, ECe was larger in 2020, except for the top and deepest soil layer (0.9 m), although differences in ECe between both years were only significant at 0.3 m depth. ESP showed a similar pattern, although in this case differences between both years were not significant for none of the studied depths. Overall, significant correlations between EC and ECe and ESP were particularly observed for the deeper soil layers and for the wettest year (2017). This result should be considered with caution since only five data points were available at each depth, although it provides evidence of the potential of EMI sensors for assessing and monitoring soil salinity/sodicity in this kind of environments.

Table 2. Descriptive statistics of ECe (dS/m) and ESP, and Pearson correlation coefficient with EC by depths.

			0.1 m	0.3 m	0.5 m	0.7 m	0.9 m
ECe	m*	2017	1.56	1.68	2.48	4.27	6.56
		2020	1.29	2.76	2.92	4.61	6.07
	T-test	p	0.28	0.03*	0.46	0.72	0.61
		med	2017	1.24	1.64	2.23	3.05
	s	2020	1.20	2.82	2.36	3.98	5.50
		2017	0.73	0.40	1.33	3.08	4.36
	CV	2020	0.36	0.44	2.16	3.13	3.66
		2017	0.47	0.24	0.54	0.72	0.66
	R	2020	0.28	0.16	0.74	0.68	0.60
		2017	-0.02	0.92	0.96	1	0.99
R	2020	-0.12	0.22	0.98	0.84	0.96	
	2017	14.55	17.52	22.70	31.67	42.88	
ESP	m*	2020	13.42	21.81	21.42	35.83	41.93
		p	0.80	0.51	0.84	0.54	0.70
	med	2017	12.64	17.41	20.09	29.78	44.81
		2020	13.27	21.56	22.33	36.05	44.66
	s	2017	8.42	3.02	12.92	15.39	15.79
		2020	1.62	8.65	5.90	6.62	13.53
	CV	2017	0.58	0.17	0.57	0.49	0.37
		2020	0.12	0.40	0.28	0.18	0.32
	R	2017	0.33	0.72	0.96	0.71	0.83
		2020	-0.06	-0.37	0.61	0.85	0.83

\*m: mean; med: median; s: standard deviation; CV: coefficient of variation; R: Pearson correlation coefficient with EC.

### 3.5. Calibration of EMI signals

Due to its anomalous behavior data from point P1 was excluded from the calibration exercise. This point is located at the headland near the service track and the drainage channel (Fig 2), where a superficial drainage tube is provisionally installed in winter to alleviate flooding, causing different hydrological conditions than in the rest of the field.

Different calibration equations were tested. The largest coefficient of determination ( $R^2$ ) between EC and ECe and ESP was found for linear equations with  $R^2$  ranging from 0.77 to 0.83 (Fig. 6).

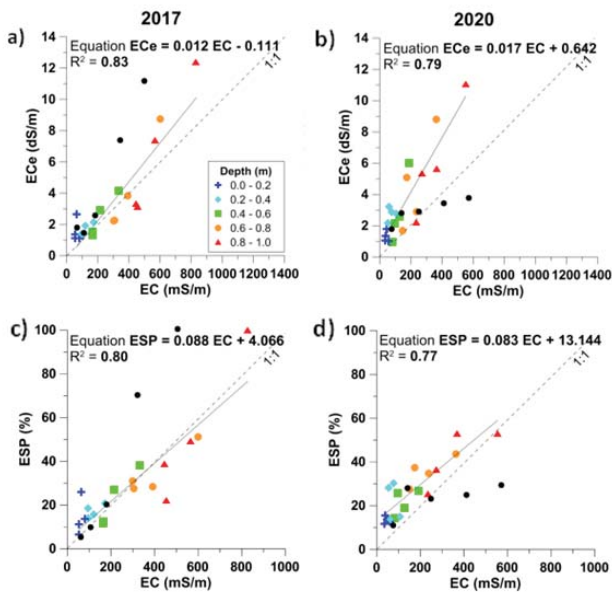


**Fig. 6.** Relationships between a) EC and saturated paste extract EC (ECe) for 2017 and b) for 2020 and between c) EC and exchangeable sodium percentage (ESP) for 2017 and d) for 2020. In black, the soil samples of P1 at different depths that were removed for fitting purposes.

These regression models were validated using the “Leave one out” Cross-Validation (LOOCV) test.

The overall result of this test is summarized in three estimators: Root Mean Squared Error (RMSE), Mean Absolute Error (MAE) and Coefficient of Determination ( $R^2$ ). The results of the LOOCV test are shown in Table 3.

**Table 3.** LOOCV test results.

EC	2017			2020		
	RMSE	MAE	$R^2$	RMSE	MAE	$R^2$
ECe	1.44	1.08	0.75	1.35	1.09	0.74
ESP	14.67	9.16	0.59	6.85	5.75	0.71

Similar results were obtained in 2017 and 2020 for ECe, but for ESP results were substantially better for 2020. Overall,  $R^2$  ranged from 0.59 (ESP 2017) to 0.75 (ECe 2017). The small ESP in 2017 could be due to the presence

of some anomalous values in view of the RMSE observed in that year.

This test verified the consistency of our models for estimating ECe and ESP from the EC values.

### 3.6. 3D evolution of ECe and ESP with depth between 2017 and 2020

Although EC was overall larger at all depths in 2017, ECe was larger in 2020, except for the 0.9 m depth. Also, larger ESP values are observed in 2020, down to approximately 0.5 m from where the trend changed (Fig. 7).

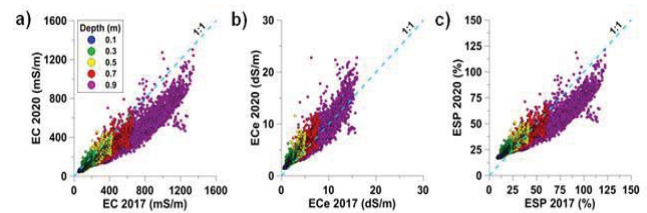


**Fig. 7.** Relationships of a) EC, b) ECe and c) ESP between 2017 and 2020 for different depths.

The larger EC values obtained in 2017, as compared to 2020 are possibly the result of a wetter soil profile in the former year, as visually observed during the soil sampling. Figure 8 shows the accumulative rainfall between 1 Sept. 2017 and 2019 and the EMI surveys in 2017 and 2020, respectively. Although the total accumulative rainfall in 2020 was larger, the rainfall event of 85 mm between days 64 and 65 caused wetter soil conditions in 2017 as compared to the survey in 2020. This might possibly have promoted the leaching of salts in 2017 down to 0.9 m where the drains are located. In contrast, in 2020, when the profile soil water content was smaller, this process may have been less pronounced, leaving larger salt contents than in 2017 in the upper soil horizons.

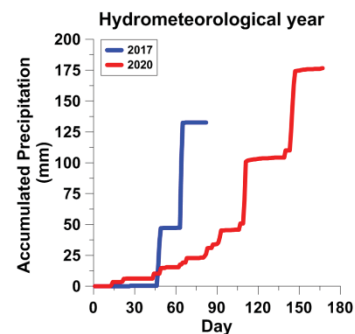


**Fig. 8.** Accumulated precipitation from the beginning of the hydrometeorological year (1 Sept.) to the date of measurement with the sensor.

From the combination of the ECe and ESP maps, soil classification maps were prepared for both years according to different salinity and sodicity levels.

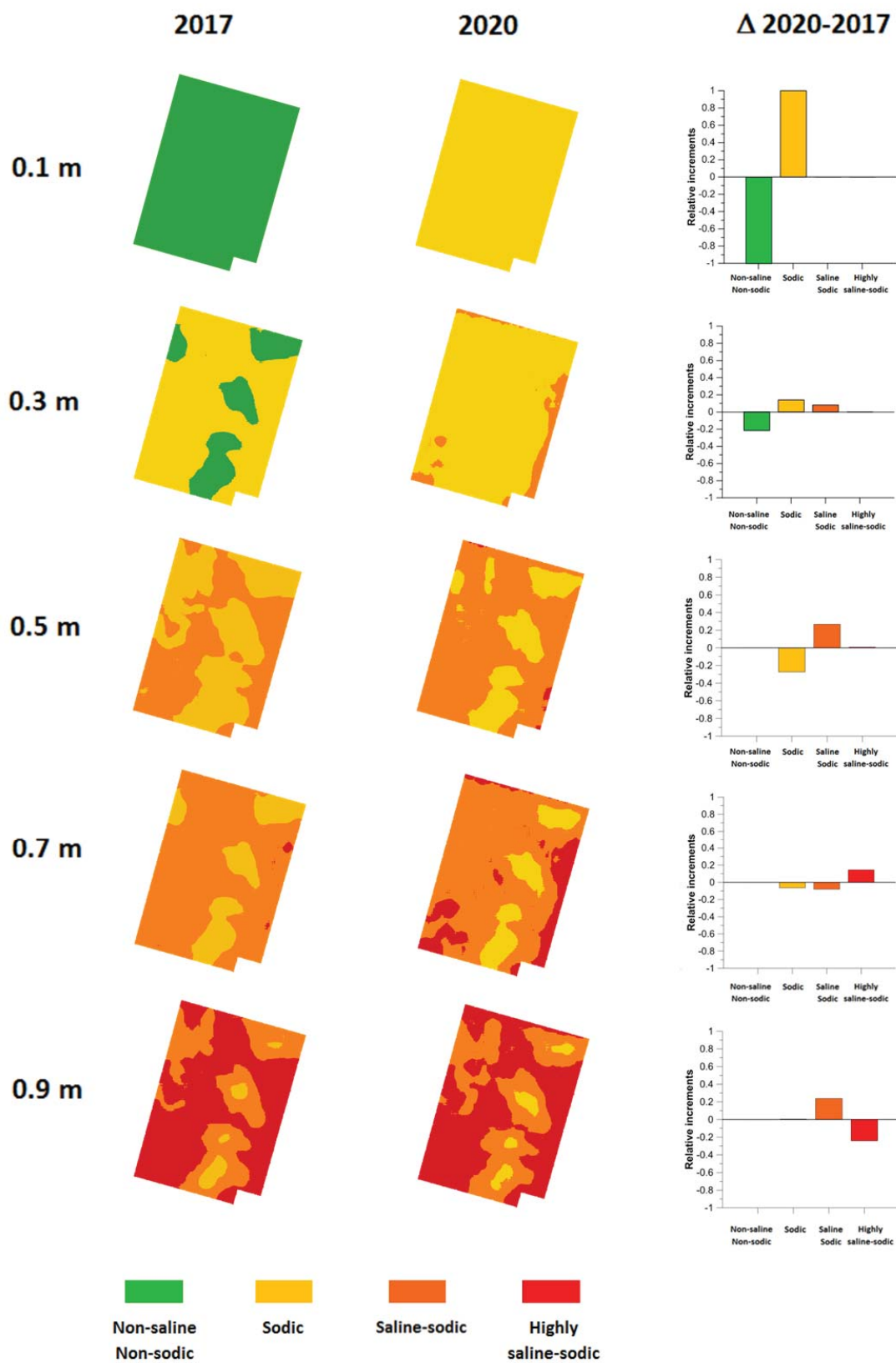


Fig. 9. Changes in salinity/sodicity classification of the study field for different depths.

The increment in the salts content between 2017 and 2020 is particularly apparent in the topsoil (Fig. 9) where the classification of the entire field changed from non-saline/non-sodic in 2017 to sodic in 2018. Changes in deeper horizons are less drastic and correspond to certain areas within the field that correspond to maximum of 20% of the total area of the field. From 0.5 m on the entire field is classified as sodic or saline-sodic, being the predominant class becomes highly saline-sodic for the deepest soil horizon. In 2020, the horizon at 0.7 m showed an evident transition between the 0.5 m and 0.9 m depths. This transition is not observable in 2017, when the presence of highly saline-sodic soil at 0.9 m is more abrupt with respect to the upper horizon. In addition, as can be seen for the horizons at 0.3 and 0.7 m in 2020, when the soil was drier, the zones that begin to change towards classifications of saline-sodic or highly saline-sodic are mainly located near the eastern edge of the field where there is a clear trend in the accumulation of salts. The effect of moisture in the soil profile is decisive for the washing of salts to the depth of the drainage network for the conservation of this agricultural soil. The changes experienced between the two years show that today the balance of these soils is very fragile and that water management here continues to be essential.

Likewise, our results indicate that the inversion of EMI values is a very powerful tool for monitoring changes in salinity and sodicity in this type of soils.

#### 4.- Conclusion

The EMI measurements were larger in 2017 than in 2020, particularly for the PRP2 signal, which explores the soil approximately down to 1m dept. This indicates larger soil apparent electrical conductivity values in 2017 than in 2020 which could be associated to higher soil salinity but also larger soil water content in 2017 as compared to 2020. Laboratory analysis of salinity/sodicity soil parameters showed however smaller values for 2017, particularly in the topsoil.

Inversion of the EMI signals for both years showed the EC changes along the soil profile from which the samples were taken. EC showed a strong correlation with the salinity/sodicity parameters, which allowed us to obtain linear calibration models for the estimation of ECe and ESP from EC, which were validated by LOOCV cross-validation.

Depth-specific EC maps were obtained through inversion for each sampling depths. The linear calibration models were used to estimate the depth-specific spatial distribution of ECe and ESP, which allowed classification of the soil according to its salinity and sodicity characteristics

Our spatio-temporal analysis in this field shows that the soil profile in 2017 was wetter than in 2020. This results in better salt leaching conditions in 2017 as opposed to the dryer conditions in 2020, leading to higher levels of soil salinity and sodicity, a trend that is maintained for all depths except for the 0.9 meter depth where the drainage

network is located and where only small differences were observed between both years with respect to the evaluated soil parameters.

Our results show that the use of EMI sensors such as DualEM-21S show a strong potential for detailed field-scale monitoring of salinity and sodicity in the soils of the B-XII irrigation district. Monitoring of soils at risk of resalinization using EMI is essential since laboratory analysis of soil samples becomes prohibitive for economic reasons.

Future work will address the reliability of the provided calibrations for the DualEM21-S sensor by evaluating their performance in other fields of the B-XII irrigation district.

*Acknowledgement.* This work is funded by the Spanish State Agency for Research through grants PID2019-104136RRC21, PID2019-104136RRC22 and PhD grant PRE2020-095133 and by IFAPA/FEDER through grant AVA2019.018.

#### 5.- References

- APHA. Standard Methods for Examination of Water and Wastewater, 17nd edn. American Public Health Association, Washington (1989).
- Assouline, S., Russo, D., Silber, A., Or, D., 2015. Balancing water scarcity and quality for sustainable irrigated agriculture. *Water Resour. Res.* 51, 3419–3436.
- Binley, A., Hubbard, S.S., Huisman, J.A., Revil, A., Robinson, D.A., Singha, K., Slater, L.D., 2015. The emergence of hydrogeophysics for improved understanding of subsurface processes over multiple scales. *Water Resour. Res.*, 51, 3837–3866.
- Kuhn et al., 2020. caret: Classification and Regression Training. R package version 6.0-86. <https://CRAN.R-project.org/package=caret>
- Corwin, D.L., Scudiero, E., 2016. Field-Scale Apparent Soil Electrical Conductivity. *Methods Soil Analysis*, Vol 1., SSSA Book Ser. 5. SSSA, Madison, WI
- Corwin, D.L., Yemoto, K., 2017. Salinity: Electrical Conductivity and Total Dissolved Solids. In: *Methods of Soil Analysis*, Vol. 2, SSSA Book Ser. 5. SSSA, Madison, WI. doi:10.2136/mta2015.0039.
- Domínguez, R., Campillo, C.D., Peña, F., Delgado, A., 2001. Effect of soil properties and reclamation practices on phosphorus dynamics in reclaimed calcareous marsh soils from the Guadalquivir Valley, SW Spain. *Arid Land Res. Manage.* 15, 203–221.
- Doolittle, J.A., Brevik, E.C., 2014. The use of electromagnetic induction techniques in soils studies. *Geoderma.* 223–225, 33–45.
- Farzadian, M., Paz, M.C., Paz, A.M., Castanheira, N.L., Gonçalves, M.C., Monteiro Santos, F.A., Triantafyllis, J., 2019. Mapping soil salinity using electromagnetic conductivity imaging—A comparison of regional and location-specific calibrations. *Land Degrad. Dev.* 30, 3317.
- González Jiménez, A., Pachepsky, Y., Gómez Flores, J.L., Ramos Rodríguez, M., Vanderlinden, K., 2021. Correcting position of delayed on-the-go field measurements by optimizing nearest neighbor statistics. In: Samper Calvete et al., *Estudios en la Zona no Saturada Vol. XV*
- Hopmans, J.W. et al., 2021. Critical knowledge gaps and research priorities in global soil salinity. *Adv. Agron.*, p.191.
- Jadoon, K.Z., Moghadas, D., Jadoon, A., Missimer, T.M., Al-Mashharawi, S.K., McCabe, F.M. 2015. Estimation of soil salinity in a drip irrigation system by using joint inversion of multicoil electromagnetic induction measurements. *Water Resour. Res.* 51, 3490–3504.
- Koganti, T., Narjary, B., Zare, E., Pathan, A.L., Huang, J., Triantafyllis, J., 2018. Quantitative mapping of soil salinity using the DUALEM-21S instrument and EM inversion software. *Land Degrad. Dev.* 29, 1768–1781.
- McLachlan, P., Blanchy, G., Binley, A., 2021. EMagPy: Open-source standalone software for processing, forward modeling and inversion of electromagnetic induction data. *Comput. Geosci.* 146, 104561.
- Moreno, F., Martín, J., Mudarra, J.L. 1981. A soil sequence in the natural and reclaimed marshes of the Guadalquivir river, Seville (Spain). *Catena*, 8, 201–211.

- Nogués, J., Robinson, D.A., Herrero, J., 2006. Incorporating electromagnetic induction methods into regional soil salinity survey of irrigation districts. *Soil Sci. Soc. Am. J.* 70, 2075–2085.
- Paz, A.M., Castanheira, N., Farzaman, M., Paz, M.C., Gonçalves, M. C., Monteiro Santos, F.A., Triantafilis, J., 2020. Prediction of soil salinity and sodicity using electromagnetic conductivity imaging. *Geoderma*, 361, 114086.
- Pedraza-Parrilla, A., Van De Vijver, E., Van Meirvenne, M., Espejo-Pérez, A.J., Giráldez, J.V., Vanderlinden, K., 2016. Apparent electrical conductivity measurements in an olive orchard under wet and dry soil conditions: significance for clay and soil water content mapping. *Precis. Agric.* 17, 531–545.
- Rhoades, J.D. Soluble salts. In *Methods of Soil Analysis*, 2nd ed.; Page, A.L., Ed.; Agronomy Monograph No 9; American Society of Agronomy, Inc.: Madison, WI, USA, 1982; Part 2; pp. 167–179.
- Triantafilis, J., Laslett, G.M., McBratney, A.B., 2000. Calibrating an electromagnetic induction instrument to measure salinity in soil under irrigated cotton. *Soil Sci. Soc. Am. J.* 64, 1009-1017.
- Triantafilis, J., Monteiro Santos, F.A. (2013). Electromagnetic Conductivity Imaging (EMCI) of Soil using a DUALEM-421 and Inversion Modelling Software (EM4Soil). *Geoderma*, 211-212: 28-38.
- U.S. Salinity Laboratory Staff, 1954. *Diagnosis and Improvement of Saline and Alkali Soils*. Handbook N° 60, Washington, DC.
- Zare, E., Huang, J., Monteiro Santos, F.M., Triantafilis, J., 2015. Mapping salinity in three dimensions using a DUALEM-421 and electromagnetic inversion software. *Soil Sci. Soc. Am. J.*, 79, 1729-1740.